Fes-deficient macrophages enhance CD8$^+$ T cell priming and tumour control through increased proinflammatory cytokine production and presentation

Brian J. Laight[1,2], Danielle Harper[1,2], Natasha Dmytryk[1,2], Shengnan Zhang[1,2] Andrew Garven[1,2], Changnian Shi[1], Richard Nauman[1,3], Jacob Kment[1,3] Faizah Alotaibi[1,2], , Yan Gao[1], Caitlyn Vlasschaert[4], David LeBrun[1,2], Kathrin Tyryshkin[2,5], David Berman[1,3], Amber Simpson[1,3,5], Charles Graham[1,3], Andrew Craig[1,3], Sameh Basta[1,3], Madhuri Koti[1,3], Peter A. Greer[1,2,3].

[1]Division of Cancer Biology and Genetics, Queen's Cancer Research Institute
[2]Department of Pathology and Molecular Medicine, Queen's University, Kingston, ON, Canada
[3]Department of Biomedical and Molecular Sciences, Queen's University, Kingston, ON, Canada
[4]Department of Medicine, Queen's University, Kingston, ON, Canada
[5]School of Computing, Queen's University, Kingston, ON, Canada

Abstract:

Cancer immunotherapy is a potent anti-cancer therapy which uses a patients own immune system to fight their cancer. Activating the immune system is crucial in successful cancer immunotherapies, various proteins, such as the Fes non-receptor tyrosine kinase exist to limit activation and maintain homeostasis. However, in cancer settings, this serves as a barrier to successful cancer immunotherapy. Here, we demonstrate the role of Fes, abundantly expressed in macrophages, as a novel innate intracellular immune checkpoint. Fes inactivity is associated with delayed tumour onset in a dose-dependent manner, and its deletion delays tumour growth, improves survival, enhances doxorubicin therapy, and sensitizes previously resistant tumours to anti-PD-1 immune checkpoint blockade. These effects are associated with an increase in Toll-like receptor signaling in antigen presenting cells, leading to an increase in proinflammatory cytokine production and T-cell capabilities. Furthermore, we demonstrate a novel role for Fes in regulating the presentation of cytokines on macrophage cell surfaces to enhance T-cell activation. Our results highlight Fes as a novel innate immune checkpoint with potential uses as predictive biomarker to effective immune checkpoint blockade, and a potential therapeutic target for successful anti-cancer immunotherapy.

Introduction:

Cancer immunotherapies employ the patient's own immune system to help reduce tumour burden, and its use in the clinic has revolutionized patient care. This is highlighted by immune checkpoint inhibitors (ICI)(1, 2) which have primarily been focussed on enhancing T cell activity through inhibiting the immune checkpoints CTLA4 and PD-1 on the surface of T cells. Unfortunately, these ICIs have not been a panacea; and the heterogeneity of tumours and variety of infiltrating immune cell types (some immunosuppressive) provides both barriers to successful cancer immunotherapy(3) and opportunities for improvement. Strategies to overcome the immune resistance exhibited by many tumour types include searching for novel immune checkpoints(4) or targeting different tumor cell types, such as cancer cells or other immune cells within the tumour microenvironment(5, 6).

One important class of immune cells involved in anti-cancer responses are antigen presenting cells (APCs), which play important roles including engulfing dying cancer cells and recruiting and priming cytotoxic T lymphocytes (CTLs). Many commonly used therapies are capable of inducing these anti-cancer immune responses, through a mechanism known as immunogenic cell death (ICD), such as anthracycline-based therapies (e.g., doxorubicin [Dox]) or radiotherapy(7). Upon induction of ICD, tumour associated antigens and damage associated molecular patterns (DAMPs) are released from dying cancer cells, activating an innate immune response in APCs which allows them to prime an anti-cancer adaptive immune response. For instance, the DNA-binding protein high mobility group box 1 (HMGB1) protein released from dying cancer cells during ICD binds to Toll-like receptor 4 (TLR) on APCs and activates a signaling cascade required for the production of pro-inflammatory cytokines(8-11). These pro-inflammatory cytokines play a crucial role in CTL priming, colloquially known as signal 3; and their absence is associated with deficient CTL effector functions and a lack of memory formation(12, 13).

Because of the importance of APCs in initiating and sustaining adaptive anti-cancer immune responses, their inhibition or polarization to an immunosuppressive phenotype makes them a potential target for modulation. While pro-inflammatory cytokine production is one of the most important functions in priming anti-cancer immune responses, uncontrolled release of these cytokines can have detrimental and even fatal consequences, such as septic shock(14), auto-immune disorder(15), or cytokine storm(16). To combat this, the human body has evolved various mechanisms to attenuate immune responses to prevent these negative consequences. One such mechanism is through the non-receptor tyrosine kinase Fes, which is abundantly expressed in APCs(17)Fes limits TLR4 signaling(18), in part through facilitating TLR4 internalization and downregulation to prevent sustained stimulation(19). Fes has also been shown to associate with MHCI and suppress inflammatory signaling in macrophages through activation of the SH2 containing protein tyrosine phosphatase-2 (SHP2)(20). While mechanisms to suppress immune cell activation, such as PD-1, are important to maintain homeostatic conditions(21), in the context of cancer these mechanisms may enable tumour growth and limit the efficacy of treatments designed to activate anti-cancer immune responses(22).

Following previous observations implicating Fes in regulation of TLR internalization(19), involvement in vesicle trafficking(23), and signalling suppression through the MHC-I axis(20), we sought to explore its involvement in regulating anti-cancer immune responses. In this study, we demonstrate that Fes serves as an innate intracellular immune checkpoint. We show that Fes-deficiency is associated with delayed tumour initiation in a genetically engineered mouse model of breast cancer, which correlates with increased immune activity within the premalignant niche. In syngeneic engraftment models of triple negative breast cancer and melanoma, Fes-deficiency was associated with delayed tumour growth and improved survival, which was further enhanced by Dox treatment and immune checkpoint blockade (ICB) therapy. Tumours in Fes-deficient mice displayed increases in activated CTLs, which correlates with sensitization of tumours to ICB therapy. This increase in CTL activation can be attributed in part to an increased T cell priming capability of *fes*$^{-/-}$ bone-marrow derived macrophages (BMDMs) compared to their wildtype counterparts, due in part to not only an increase in signal 3 cytokines production,

namely interleukin-12 (IL-12), but also to the method of IL-12 presentation to CTLs through IL-12 membrane retention on the APCs. Taken together, these results demonstrate a novel role for Fes as an immune checkpoint, and a potential predictive biomarker for successful ICB therapy.

Results:

Fes-deficiency delays tumour growth in a gene dose-dependent manner and is associated with increased immune infiltration in a transgenic mouse model of Her2+ breast cancer.

We previously showed that Fes-deficiency is associated with delayed tumour growth in an immunodeficient mouse engraftment model which lacks B and T cells(24). While that study implicated Fes-expressing macrophages in the modulation of tumourigenesis, we could not assess potential roles in the regulation of adaptive immunity. Here we have explored this question using immune competent models, beginning with a *MMTV-Neu* transgenic mouse model of HER2+ mammary tumourigenesis(25) crossed with transgenic mice targeted with a kinase-inactivating K588R knock-in mutation in *fes* (fes^{KR}). While the average tumour onset time in $fes^{+/+}$ mice was 274 days, that was delayed to 316 days in $fes^{KR/+}$ and 389 days in $fes^{KR/KR}$ mice (Fig. 1A). These results demonstrated that a functional inhibition of 50% was sufficient to delay tumour onset, and that was even further delayed in mice lacking any Fes kinase activity. Interesting, once palpable tumours were detected, their growth rates were indistinguishable, suggesting tumour initiation had overcome some sort of suppression (Supplemental Figure 1A). This observation correlates with a small magnitude, but significant effect of a single nucleotide polymorphism in human *FES* associated with differential Fes protein levels (rs17514846)(26), which predicts that higher Fes levels are correlated with higher cancer incidence rates (HR 1.03 [1.01 – 1.05], p=0.01) and risk of death (HR 1.06 [1.01 – 1.11], p=0.03) for those without cancer at baseline in the United Kingdom Biobank cohort of over 400,000 individuals.

To directly explore a potential role of the immune system on this delay in tumour onset, we isolated pre-malignant mammary glands (before palpable tumours could be detected) and performed immunohistochemical staining to assess the presence of myeloid and T cells. We found that there was an increase in both CD11b+ (Fig 1B) and CD3+ cells in $fes^{KR/KR}$ glands (Fig.1C). We also observed a decrease in Ki67+ proliferating epithelial cells in the $fes^{KR/KR}$ glands (Fig 1D), showing a reduction in proliferation of mammary epithelial cells. Immunoblotting analysis of mammary gland lysates revealed an increase in phosphorylated NFκB in $fes^{KR/KR}$ mice (Fig 1E); an important transcription factor for inflammatory signaling, including the expression of Signal 3 cytokines. Finally, an increase in immune cell infiltration was also apparent after tumours formed, where there was an increase in immune cell content relative to tumour volume (Fig 1F).

Fes-deficient mice have improved survival and delayed tumour growth in the presence or absence of doxorubicin treatment.

In the *MMTV-Neu* transgenic tumour-onset model, we saw that a reduction in functional Fes was associated with delayed tumour onset and an increase in immune cell infiltration and NFκB

phosphorylation. This suggested a role for Fes in the regulation of anti-tumour immunity. To further explore this, we employed the E0771 mammary carcinoma and B16F10 melanoma syngeneic orthotopic engraftment models using C57BL/6 mice targeted with a *fes* null mutation (*fes*$^{-/-}$) or wild type (*fes*$^{+/+}$) mice. Dox treatment was used in these studies to induce ICD and promote innate and adaptive anti-tumour immunity (Fig 2A,D). Tumour growth was significantly slower in *fes*$^{-/-}$ mice with or without Dox treatment, and Dox was more effective in *fes*$^{-/-}$ than *fes*$^{+/+}$ mice in both models (Fig 2B,E). Without Dox treatment, survival was significantly longer in *fes*$^{-/-}$ compared to *fes*$^{+/+}$ mice in both models (Fig 2C,F). Dox treatment prolonged survival of *fes*$^{-/-}$ mice in both models, but in *fes*$^{+/+}$ mice Dox treatment only improved survival in the B16F10 model. These observations are consistent with a Fes effect driven by the tumour immune microenvironment. Furthermore, neither E0771 nor B16F10 cells express detectable levels of Fes (Data not shown).

Fes-deficiency is correlated with an increased anti-tumoural immune microenvironment, enhanced by doxorubicin therapy.

Fes deficiency in cancer cell engraftment recipients was associated with slower tumour growth without treatment, and an additional delay in tumour growth and increased survival when treated with Dox (Fig. 2). These observations, coupled with delayed tumour onset and increased myeloid and T cell infiltration and NFκB activation in the pre-malignant niche of a Fes-deficient transgenic model of breast cancer (Fig.1), implicate Fes in regulating an anti-cancer immune response. This led us to next explore the tumour immune profiles of the E0771 and B16F10 engraftment models in *fes*$^{+/+}$ or *fes*$^{-/-}$ mice with or without Dox treatment (Fig 3A,H). There were no differences in the frequency of tumour associated CD8^{+} T cells (CTLs) (Fig 3B,I), or splenic CTLs (Supplemental Fig 2A,K) in either engraftment model and no differences in tumour associated CTL activation (CD69^{+}) between untreated and Dox treated *fes*$^{+/+}$ mice (Fig 3C,J). However, there was an increase in tumour associated CTL activation in untreated *fes*$^{-/-}$ mice compared to both treated and untreated *fes*$^{+/+}$ mice in both models, which was further enhanced by Dox treatment (Fig 3C,J). In the spleens, *fes*$^{-/-}$ mice had higher levels of CTL activation (especially in the melanoma model), but this was not elevated by Dox treatment with either genotype or model (Supplemental Fig 2B,E). Increased tumour associated CTL PD-1 positivity (indicative of more extensive and prolonged activation), was seen in *fes*$^{-/-}$ mice with Dox treatment in both models (Fig 3D,K). PD-1 positivity was inducible by Dox treatment in EO777 tumours only in *fes*$^{-/-}$ mice (Fig 3E); but was already higher in the B16F10 model in *fes*$^{-/-}$ mice without Dox treatment and was not further induced by Dox treatment (Fig 3K). In the spleen, there was a Dox-induced increase in PD-1 positivity only in *fes*$^{+/+}$ treated animals with the E0771 model (Supplemental Fig 2C,F).

We next looked at the frequency of tumour associated macrophages and saw no *fes* genotype associated differences in either model (Fig 3E,L). However, we observed a *fes* genotype associated shift from immunosuppressive M2 (CD206^{+}) macrophages (Fig 3F,M) to proinflammatory (CD206^{-}/CD80^{+} and/or MHCII^{+}) M1 macrophages (Fig 3G,N) in *fes*$^{-/-}$ mice in both engraftment models. This shift to more pro-inflammatory and less immunosuppressive macrophages was also seen in the spleen (Supplemental Fig 2G-L). In both E0771 and B16F10

tumors, we saw no *fes* genotype associated changes in dendritic cell (DC) numbers (Supplemental Fig 2G,Q). However, in the E0771 model, we observed an increase in DC activation in tumours in *fes*$^{-/-}$ mice (Supplemental Fig 3H), but this was not observed in the B16F10 model (Fig 3Q). These results demonstrate that Fes deficiency is associated with increased CTL activation and PD-1 positivity, as well as an increase in pro-inflammatory M1 macrophages and decrease in immunosuppressive M2 macrophages in the tumor.

Fes deficient macrophages have increased TLR signaling, pro-inflammatory cytokine production and enhanced T cell priming functionality.

Fes displays tissue-specific expression, with highest levels observed in immune cells, primarily macrophages, DCs, as well as NK and B cells; but Fes is not expressed in T cells (Supplemental Fig 2B). Since we see *fes* genome associated changes in the phenotype of tumour associated macrophages in both tumour models, we decided to explore the role of Fes in antigen presenting cells; specifically, macrophages since they made up most of the APCs within the tumour.

We have previously shown that Fes plays a role in downregulating inflammatory signaling in macrophages, in part through promoting LPS-induced endocytosis and downregulation of the TLR4 receptor, which suppresses TNFα expression(18). Additionally, it has been shown that Fes participates in suppressing inflammatory signaling in macrophages through association with MHC-I and phosphorylation of SHP2, which leads to suppression of TBK1 and NFκB pathways responsible for inflammatory cytokine expression(20). Here we explored the effects of Fes deficiency on the LPS-TLR4 signaling pathway in macrophages. To do this, we isolated BMDMs from *fes*$^{+/+}$ and *fes*$^{-/-}$ mice, treated them with 1μg/mL LPS and looked at downstream signaling. The *fes*$^{-/-}$ BMDMs displayed earlier and more robust activating phosphorylation of NFκB (Fig 4A,B), TBK1 (Fig 4A,C), and IRF3 (Fig 4A,D) compared to *fes*$^{+/+}$ BMDMs. For pSHP2 however, we saw that at baseline, there was almost a 2-fold increase in SHP2 phosphorylation, but following stimulation, pSHP-2 in both genotypes were equal (Fig 4A,E). We also observed increased NFκB and TBK1 phosphorylation in *fes*$^{-/-}$ bone marrow derived DCs compared with *fes*$^{+/+}$ DCs after LPS stimulation (Supplemental Fig 4A-C). The *fes*$^{-/-}$ BMDMs were also more sensitive to LPS stimulation than *fes*$^{+/+}$, with increased NFκB and TBK1 phosphorylation even at concentration as low as 300pg/mL (Supplemental Fig 4D-F).

Seeing that Fes deficiency is associated with enhanced LPS-induced phosphorylation of NF-κB and TBK1, which play key roles in transcriptional upregulation of inflammatory cytokine genes, we next performed bulk RNAseq on *fes*$^{+/+}$ or *fes*$^{-/-}$ BMDMs before or after stimulation with LPS for 4 hours and performed a GO analysis on differentially expressed genes that met the following criteria: (1) were LPS inducible; (2) had at least a 1.25 fold increase in gene expression in LPS stimulated *fes*$^{-/-}$ compared to *fes*$^{+/+}$ BMDMs; and (3) the fold change associated with LPS stimulation was greater in *fes*$^{-/-}$ compared to *fes*$^{+/+}$BMDMs. The differentially expressed genes emerging from this analysis were significantly associated with increased inflammatory pathway activation and cytokine production, most specifically IL-12 and T cell activation pathways (Fig 4F), which was confirmed by looking at the fold change of several key genes following LPS stimulation (Fig 4G). Next, to correlate RNA expression changes with protein, we looked at the

secreted levels of 13 cytokines from LPS treated BMDMs, and found that 11 of 13 cytokines were increased from *fes*$^{-/-}$ BMDMs (Fig 4H-K; Supplemental Fig 4H-P) compared to *fes*$^{+/+}$, most notably four important immunostimulatory cytokines TNFα (Fig 4H), IL-6 (Fig 4I), IL-12 (Fig 4J), and IFNβ (Fig 4K). Since IL-12 had the largest increase in RNA expression, but had relatively low secreted levels, we analyzed cell-associated IL-12 on LPS stimulated BMDMs. We found that *fes*$^{-/-}$ BMDMs had increase IL-12 positivity compared to fes$^{+/+}$ (Fig 4L) in the absence of Brefeldin A (something that is required for assessing other cytokines such as TNFα(supplemental Fig 4Q)); and interestingly, this difference was even more apparent if the flow cytometry was restricted to assessing IL-12 on the external surface of nonpermeabilized cells (Fig 4M), suggesting that Fes plays a role in the trafficking of IL-12.

These increases in TLR4 signaling, pro-inflammatory cytokine gene expression, and IL-12 on the surface of *fes*$^{-/-}$ BMDMs suggest that Fes deficient macrophages might be more effective at priming CTLs than their wildtype counterparts. To explore this, we pulsed *fes*$^{+/+}$ or *fes*$^{-/-}$ BMDMs with 10^{-10}M SIINFEKL peptide and stimulated them with either the TLR4 agonist LPS (1µg/mL) or the TLR1/2 agonist Pam3Cys (0.1µg/mL) before co-culturing with splenic OT-1 CD8+ T cells in a 1:1 ratio. The *fes*$^{-/-}$ BMDMs activated a greater percentage of CD8^{+} T cells both with and without LPS (Fig 4J) or Pam3Cys stimulation (Fig 4L). The *fes*$^{-/-}$ BMDMs also primed these CD8^{+} T cells to a greater extent than *fes*$^{+/+}$ BMDMs in the presence of LPS (Fig 4K) and Pam3Cys (Fig 4M), as determined by the higher levels of IFNγ. This more efficient T cell priming by *fes*$^{-/-}$ BMDMs was preserved across a range of SIINFEKL concentrations (Supplemental Fig 4S-U) and showed no priming in the absence of SIINFEKL peptide (Supplemental Fig 4V). However, there was no apparent *fes* genome associated difference in the ability of BMDMs to present the SIINFEKL peptide on MHCI (Supplemental Fig 4V)

Fes-deficiency in BMDMs enabled them to prime CTLs more efficiently and to a greater extent, suggesting Fes-deficiency in APCs may allow them to promote more effective adaptive immunity in both tumour models. To directly show this, we performed adoptive macrophage transfer experiments with either *fes*$^{+/+}$ or *fes*$^{-/-}$ IFNγ-treated BMDMs injected directly into B16F10 engraftment tumours in *fes*$^{+/+}$ mice. Both *fes*$^{+/+}$ and *fes*$^{-/-}$ BMDMs reduced B16F10 tumour weights compared to mock injections with PBS, but *fes*$^{-/-}$ BMDMs were more effective at reducing tumour weights than *fes*$^{+/+}$ BMDMs (Fig 4N).

Tumours in Fes deficient mice are more sensitive to PD-1 therapy.

In light of our observation of increased PD-1 positivity on tumour associated CTLs in *fes*$^{-/-}$ mice with both engraftment models (Fig 3D,K), we decided to explore the effect of PD-1 therapy. Since CTLs in the E0771 model only show an increase in PD-1 positivity following Dox therapy, we treated all mice with Dox, and either an isotype antibody control (IgG) or anti-PD-1 antibody (Figure 5A, D). In both the E0771 and B16F10 models, Dox, and anti-PD-1 treated *fes*$^{+/+}$ mice show a decrease in tumour growth (Figure 5B, E), but no improvement in survival (Figure 5C, F) compared to Dox therapy alone, consistent with literature describing these tumour types as anti-PD-1 therapy resistant(27-32). Impressively, *fes*$^{-/-}$ mice treated only with Dox performed just as well (Fig 5B), or better (Fig 5E) than *fes*$^{+/+}$ treated with both Dox and anti-PD-1 therapy on delaying tumour growth. While anti-PD-1 therapy in *fes*$^{+/+}$ mice provided only a minimal tumour

delay and no survival advantage, anti-PD-1 treated *fes*$^{-/-}$ mice demonstrated greater tumour delay and a greater survival advantage compared to all other treatment groups (Fig 5B,C,E,F). These observations demonstrated that Fes deficiency sensitizes these anti-PD-1 therapy resistant tumour types to this ICB treatment.

Discussion:

Here we provide novel evidence that the Fes non-receptor tyrosine kinase plays an intracellular innate immune checkpoint role in APCs that modulates anti-cancer adaptive immunity in part by regulating expression and presentation of the pro-inflammatory signal 3 cytokine IL-12 to CTLs. We show in a transgenic mouse breast cancer model that germline inactivating mutation in *fes* is associated with a delay in tumour onset. These *fes*$^{-/-}$ mice also displayed delayed tumour growth, enhanced Dox efficacy and improved response to anti-PD-1 ICB treatment in engraftment models of triple negative breast cancer and melanoma; and this correlated with increased T cell activation within the tumour and with increased pro-inflammatory signaling and IL-12 production in *fes*$^{-/-}$ macrophages.

In the transgenic tumour onset model, we see increased immune infiltration of CD3 and CD11b positive cells and inflammatory signaling (pNF-kB) correlating with delay in tumour onset. Inflammation can be a double-edged sword, where in some contexts it can induce tumour initiation and growth (chronic inflammation), and in others it can suppress tumour initiation and growth (acute inflammation) (33-35). It is well established that the immune system can suppress tumourigenesis until the cancer overcomes this through induction of immunosuppression(36). We first saw evidence that Fes might participate in immunosuppression in the transgenic tumour onset model, where delayed tumour onset correlated with increased density of CD3 and CD11b immune cells in the mammary glands prior to detection of palpable tumours in mice with targeted kinase-inactivating mutations in *fes*. However, once tumours were detected, their growth rates were the same across mouse *fes* genotypes, potentially demonstrating an adaptation of malignant cells to the tumour suppression. This could potentially explain the reduction in tumour incidence of people harbouring the rs17514846 SNP, which reduces Fes expression by ~50%(26).

Using BMDMs we demonstrated that *fes*$^{-/-}$ macrophages had increased inflammatory signaling as seen by the increase in phosphorylated (activated) NFκB and TBK1 downstream of TLR4 engagement by LPS. TBK1 goes on to phosphorylate and activate Interferon response factor 3 (IRF3). Activated IRF3 and NFκB are crucial for signal 3 cytokine production (e.g., type I IFNs and IL-12)(37). This was confirmed by RNAseq analysis showing that important signal 3 cytokines were transcriptionally upregulated following LPS stimulation to a higher degree in *fes*$^{-/-}$ compared to *fes*$^{+/+}$ BMDMs. Important signal 2 co-stimulatory molecules such as CD80, TL1A(38-40), and CD40(41, 42), were also expressed to higher levels in *fes*$^{-/-}$ BMDMs both in the presence and absence of LPS. These results may explain increased T cell activation by *fes*$^{-/-}$ BMDMs in the co-culture assay in the absence of LPS. The presence of increased co-stimulatory proteins and the enhanced sensitivity of *fes*$^{-/-}$ macrophages to respond to very low levels of LPS may potentially explain the already present increase in T cell activation in both E0771 and B16F10 models, and the ability for suboptimal induction of ICD to increase T cell activation in

both models. During uninhibited tumour growth, there is still a degree of cell death that occurs(43, 44), which may produce sufficient DAMPs to activate innate immunity in *fes*$^{-/-}$ mice, but not *fes*$^{+/+}$ mice. This is supported not only by the increased sensitivity of *fes*$^{-/-}$ BMDMs to low concentrations of LPS, but also the enhanced CTL priming functionality at low antigen levels. This may also explain how tumour initiation was delayed in the MMTV-Neu model, as the mice harbouring *fes* kinase-inactivating mutations not only had more CD11b myeloid cells within the premalignant glands, but macrophages or DCs among these cells may have had increased anti-cancer APC functionality. Additionally, the apparent increased functionality of *fes*$^{-/-}$ BMDMs over *fes*$^{+/+}$ was shown in the adoptive macrophage transfer. Cells from both genotypes were polarized to a proinflammatory phenotype by IFNγ stimulation; and while both genotypes reduced tumour volumes, the effect was greater in the mice which received *fes*$^{-/-}$ BMDMs. Given the results of the *in vitro* BMDM/T cell co-culture priming experiments, it is likely this improved tumour growth control was due to increased *in vivo* inflammatory cytokine presentation and T cell priming capabilities.

In BMDMs, IL-12-expressing *fes*$^{-/-}$ BMDMs were more abundant compared to *fes*$^{+/+}$, but what was most striking was the LPS-induced increase in membrane retained IL-12 in *fes*$^{-/-}$ BMDMs, which was not observed in *fes*$^{+/+}$ BMDMs. Not only were there more *fes*$^{-/-}$ cells expressing IL-12 on their surface, but the amount of IL-12 expressed on the surface, as determined by IF in the T cell co-culture assays, was also increased. This increase in cell-surface IL-12 may be partially responsible for improved T cell priming by *fes*$^{-/-}$ BMDMs. One group demonstrated that increased membrane-associated IL-12 improved DC-mediated priming of OT-II T cells, despite an apparent reduction in secreted IL-12(45). This suggests that membrane-associated IL-12 may be more important than secreted IL-12 in stimulating T cells. This provides a potential novel mechanism by which Fes might regulate T cell priming; by not only suppressing the expression of IL-12 following TLR stimulation, but also by promoting IL-12 secretion through a role in vesicular trafficking. Fes was previously reported to colocalize in the Golgi, as well as within cytoplasmic vesicles involved in both the endocytic and exocytic pathways(23). This is significant as IL-12 has also been shown to associated with Rab7 in late endosomes, and the deletion of the SNARE VAMP7, which is involved in exocytosis, caused a decrease in secreted IL-12(46). Future studies will be needed to explore potential trafficking interactions between Fes and IL-12 within APCs. Interestingly, the Fes-related kinase Fer has been shown to regulate ligand induced internalization of the EGFR(47), while Fes was implicated in regulating LPS-induced internalization of TLR4(19). These observations provide president for a role for this class of non-receptor tyrosine kinases in trafficking of signaling proteins.

Finally, an important finding for potential clinical applications is the effect of Fes deficiency on sensitivity to anti-PD-1 therapy. Immune checkpoint therapy has become one of the most widely used therapies in cancer, with over 1500 clinical trials using anti-PD-1 antibodies, and their approval as first-line treatment in certain cases (such as metastatic melanoma), and being used in TNBC in combination with chemotherapy in certain contexts (48). Metastatic melanoma has a response rate of ~32.6 – 45%, which represents one of the biggest successes of ICI therapy (49-51). Unfortunately, the response rate in TNBC remains low, from 5% in previously treated patients(52), up to 21% for first line therapy(53, 54). The combination of PD-1 therapy with

chemotherapy shows improvements ranging from 25.8%(55), up to 64.8%(56) (albeit addition of PD-1 therapy improved outcomes by only 13.6% compared to chemotherapy alone). These results demonstrate that there is still significant room for improvement using combined chemoimmunotherapy. Another group showed that ICD induction with Dox, followed by Nivolumab treatment results in a response rate of 35%, but most interestingly showed an increase in gene expression of immune-related genes involved in PD-1-PD-L1 and T cell cytotoxicity pathways(57). This reprogramming of the tumour microenvironment to one that is more inflamed and anti-tumoural, was recapitulated in our study, which showed increased T cell activation and PD-1 expression in *fes*$^{-/-}$, but not *fes*$^{+/+}$mice. Furthermore, E0771 and B16F10 models are commonly reported in the literature as resistant to anti-PD-1 therapy(27-32, 58-60). This was seen in our studies where even in combination with Dox, anti-PD-1 elicited only a marginal improvement on tumour growth, and no improvement on survival in *fes*$^{+/+}$ mice in either model. However, the combination of Dox and anti-PD-1 therapy in *fes*$^{-/-}$ mice conferred a greater delay in tumour growth and a significant increase in survival compared to Dox alone. This demonstrated that host Fes-deficiency sensitizes these tumours to anti-PD-1 therapy, most likely because of increased T cell activation and PD-1 positivity seen in *fes*$^{-/-}$ tumours at baseline and following Dox therapy. This is reminiscent of the aforementioned combined chemotherapy plus PD-1 study of metastatic triple negative breast cancer which was reported in the TONIC clinical trial(57). These results highlight Fes as both a potential therapeutic target as well as a predictive biomarker for successful ICB.

Future work aims to explore the molecular mechanisms through which Fes regulates IL-12 expression, trafficking, secretion, or presentation on the APC surface; correlating myeloid-specific Fes expression with patient outcomes through publicly available outcome data; and developing a novel and specific inhibitor for Fes with limited off-target effects. Currently, the ALK inhibitor Lorlatinib, developed for use in non small cell lung cancer has been shown to have off-target effects of inhibiting Fes and several other kinases(61). Due to this, an approach to selectively target Fes will be required.

In our study, we have shown that the non-receptor tyrosine kinase Fes, plays an important role in mediating successful anti-cancer immunotherapy. We believe that Fes falls into a novel group of immune checkpoints, we have coined as an innate intracellular immune checkpoint. Its deletion or inactivation leads to an increase in anti-tumour immune cell infiltration and activation within the tumour. This change in immune cell composition of the tumour correlates with increased tumour control and survival in both triple negative breast cancer and melanoma models, as well as sensitizing both models to additional anti-PD-1 ICB therapy, showing the role of Fes as a tumour agnostic checkpoint and identifying it as both a predictive biomarker for ICB therapy success, and an attractive therapeutic target.

Figure Captions:

Fig 1: Delay in tumour onset associated with *fes* inactivation and increased inflammation and immune infiltration into pre-malignant niche. (A) MMTV-Neu transgenic mice were crossed with either $fes^{+/+}$ mice (n=46), or with mice harbouring one ($fes^{KR/+}$) (n=47) or two ($fes^{KR/KR}$) (n=49) kinase-dead alleles, and tumour onset was assessed through manual palpation. Representative immunohistochemistry images and quantification of (B,C) CD3 staining in $fes^{+/+}$ (n=6) or $fes^{KR/KR}$ (n=6) mice or (D,E) CD11b staining in $fes^{+/+}$ (n=3) or 3 $fes^{KR/KR}$ (n=3) mice. (F) Pre-malignant glands were isolated from $fes^{+/+}$ (n=5) or $fes^{KR/KR}$ (n=5) mice and probed for pNFκB through western blot analysis. (G) Mammary glands containing similarly sized tumours were harvested from either $fes^{+/+}$ (n=11) or $fes^{KR/KR}$ (n=24) mice, stained with H&E, and were assessed by a blinded pathologist to assess stromal immune grading. Time-to-event (A) statistics were assessed through Log-rank (Mantel-Cox) test, and IHC and western blot statistical analysis was performed through an unpaired one-tailed t-test; *p<0.05, **p<0.01, ***p<0.001, ****p<0.0001.

Fig 2: Fes deficiency delays tumour growth, enhances survival, and improves doxorubicin effectiveness in a tumour agnostic manner. Schematic of the tumour growth and survival experiment for **(A)** E0771 and **(B)** B16F10 models. **(C,E**) E0771 cells or **(D,F)** B16F10 were orthotopically engrafted into either $fes^{+/+}$ or $fes^{-/-}$ mice (female for E0771 and male for B16F10), and treated with either 5% DMSO, or 5mg/kg Dox in the E0771 model, or 2.5mg/kg in the B16F10 model and were monitored using calipers to an endpoint of 1.1cm^3 or physiological endpoint (e.g., ulceration) (**C,D**) and survival plotted **(E,F)**. Data represented as tumour volumes ± SEM of two independent experiments of both E0771 and B16F10 models with the following numbers of animals per group, respectively: $fes^{+/+}$ + DMSO (E0771 n=9, B16F10 n=10), $fes^{+/+}$ + Dox (E0771 n=10, B16F10 n=13), $fes^{-/-}$ + DMSO (E0771 n=9, B16F10 n=11), $fes^{-/-}$ + Dox (E0771 n=11, B16F10 n=12). Differences between tumour growth results were analyzed by two-way ANOVA with Tukey's multiple comparisons test and survival data was analyzed using Log-rank (Mantel-Cox) test; * p<0.05, ** p<0.01, *** p<0.001, ****p<0.0001.

Fig 3: Fes deficiency promotes a shift to an anti-tumour microenvironment and sensitizes tumours to doxorubicin-induced T cell activation. Schematic representation of immune profiling of **(A)** E0771 or **(H)** B16F10 tumours. Tumours were dissociated and stained for **(B,** E0771 n=14**; I,** B16F10 n=5) CD8+ T cells (CD45+, CD3+, CD8+; CTLs), **(C,** E0771 n=14; **J,** B16F10 n=5**)** CD69+ CTLs, **(D,** E0771 n=14; **K,** B16F10 n=5**)** PD-1+ CTLs, **(E,** E0771 n=18; **L,** B16F10 n=5**)** macrophages (CD45+, CD11b+, F4/80+), **(F,** E0771 n=18; **M,** B16F10 n=5**)** M2 macrophages (CD206+), **(G,** E0771 n=18**; N,** B16F10 n=5 **)** M1 macrophages (CD206-, MHCII+ and/or CD80+) and analyzed by flow cytometry. Results were analyzed by one-way ANOVA with Tukey's multiple comparisons test; * p<0.05, ** p<0.01, *** p<0.001, **** p<0.0001.

Fig 4: Fes deficiency is associated with a pro-inflammatory phenotype in bone marrow derived macrophages that correlates with enhanced T cell priming and tumour control through improved IL-12 signaling. (A-E) Bone marrow derived macrophages (BMDMs) were isolated from either $fes^{+/+}$ (n=5) or $fes^{-/-}$ (n=5) mice and stimulated with 1µg/mL LPS for the indicated time points before lysis and probing for (A) Fes, pNFκB, pTBK1, pIRF3 pSHP2 and

GAPDH. Densitometry was assessed using ImageJ, and results were normalized to the band with the greatest density for either (B) pNFκB (C) pTBK1, (D) pIRF3, or (E) pSHP2 of the *fes*$^{+/+}$ BMDMs. **(F,G)** RNA was isolated from either *fes*$^{+/+}$ (n=3) or *fes*$^{-/-}$ (n=3) BMDMs that were either untreated or treated with 1µg/mL of LPS for 4 hours for bulk RNA sequencing. Total RNA was isolated using TRI Reagent (Sigma-Aldrich) and synthesized into cDNA. cDNA was sent for poly-A enriched RNA sequencing and alignment to the GRCm38 (Ensembl 102 release) murine genome. **(H-K)** BMDMs from either genotype (n=5) were left untreated or stimulated with 1µg/mL LPS for either 4, 8 or 12hrs. The supernatants were collected, spun at 10,000rpm at 4ºC for 15 minutes to pellet any cell debris, and assessed for cytokine secretion using the BioLegend Mouse Inflammation LEGENDplex panel. BMDMs of either genotype (n=3) were treated with LPS for 8 or 24hrs, before staining for (**L**) cell surface IL-12 (staining in the absence of permeabilization) or (**M**) total IL-12 (following permeabilization). (**N-Q**) BMDMs were pulsed with 10^{-10}M SIINFEKL peptide for 2 hours, washed, stimulated with (**N**, *fes*$^{+/+}$ n=9 and *fes*$^{-/-}$ n=10; **O,** n=6) 1µg/mL LPS or (**P,** n=6; **Q,** n=6) 0.1µg/mL Pam3Cys for 1 hour. Following another wash, OT-1 T cells were added to the macrophage culture in a 1:1 ratio for a total of 6 hours, with 5µg/mL Brefeldin A added after 2 hours. Cells were then analyzed for (N,P) intracellular IFNγ positivity and (O,Q) IFNγ median fluorescence intensity (MFI). **(R)** 6e4 B16F10 cells were orthotopically engrafted in *fes*$^{+/+}$ mice and when tumours reached 100mm^3, were injected intratumourally with either PBS, or 3e6 *fes*$^{+/+}$ or *fes*$^{-/-}$ M1 polarized BMDMs. Nine days later, mice were euthanized, and tumours weights assessed, and normalized to the PBS control group. Figures B-E, H-Q were analyzed two-way ANOVA with Sidak's multiple comparisons test. Figure R was assessed by one-way ANOVA with Tukey's multiple comparisons test; * $p<0.05$, ** $p<0.01$, *** $p<0.001$, **** $p<0.0001$.

Fig 5: Fes deficiency enhances anti-PD-1 therapy and sensitizes previously resistant tumours. Schematic of tumour growth and survival using **(A)** E0771 and **(B)** B16F10 models. **(C,E)** E0771 cells or **(D,F)** B16F10 were orthotopically engrafted into either *fes*$^{+/+}$ or *fes*$^{-/-}$ mice (female for E0771 and male for B16F10), and all mice were treated with either 5mg/kg Dox (E0771 model), or 2.5mg/kg Dox (B16F10 model), and treated with either 200µg IgG antibody control, or 200µg anti-PD-1 antibody. Tumour growth (B,E) was monitored using calipers to an endpoint of 1.1cm^3 or humane endpoint (e.g., ulceration) and survival plotted (C,F). Data were represented as tumours volumes ± SEM of two (B16F10) or three (E0771) independent experiments with the following numbers of animals per group, respectively: *fes*$^{+/+}$ + Dox + αIgG (E0771 n=15, B16F10 n=12), *fes*$^{+/+}$ + Dox + αPD-1 (E0771 n=15, B16F10 n=12), *fes*$^{-/-}$ + Dox + αIgG (E0771 n=16, B16F10 n=13), *fes*$^{-/-}$ + Dox + αPD-1 (E0771 n=16, B16F10 n=14). Tumour growth results were analyzed by two-way ANOVA with Tukey's multiple comparisons test and survival data was analyzed using Gehan-Breslow-Wilcoxon Test for survival; * $p<0.05$, ** $p<0.01$, *** $p<0.001$, **** $p<0.0001$.

Supplemental Figure Captions:

Supplemental Figure 1: Tumour growth rates and representative IHC images, and pNFkB tumour immunoblot. (**A**) *fes*$^{+/+}$, *fes*$^{+/KR}$, or *fes*$^{KR/KR}$ mice were crossed with MMTV-Neu transgenic mice, and monitored for tumour initiation by physical palpation, after tumours volumes were assessed weekly by caliper measurements, and tumor growth rate was calculated as a function of mm^3 per day. **(B-D)** Representative images of CD11b, CD3, and Ki67 immunohistochemistry (IHC) staining. **(E)** Tumours from either *fes*$^{+/+}$ or *fes*$^{-/-}$ were isolated and homogenized in RIPA buffer. Cell debris was then pelleted out and supernatant was probed for pNFκB and Tubulin. **(F)** Representative Hematoxylin and eosin (H&E) IHC staining.

Supplemental Figure 2: Fes is expressed in bone marrow derived macrophages (BMDMs), B cells, and NK cells, but not T cells. (**A**) Flow plots of negative isolation of T cells, NK cells, and B cells. **(B)** Total splenocytes, BMDMs, negatively isolated T cells, negatively isolated B cells, negatively isolated NK cells, E0771 cells and B16F10 cells were lysed in RIPA buffer and probed for Fes and GAPDH by immunoblot analysis.

Supplemental Figure 3: Representative immune profiling flow plots and splenic and tumour immune profiling. (A) Representative flow cytometry plots for CD8$^+$ T cell immune profiling. **(B)** Representative flow cytometry plots for macrophage and dendritic cell immune profiling. Spleens were dissociated and stained for **(C, M**) CD8+ T cells (CD45+, CD3+, CD8+; CTLs), **(D, N)** CD69+ CTLs, **(E, O)** PD-1+ CTLs, **(F, P)** macrophages (CD45+, CD11b+, F4/80+), **(G, Q)** M2 macrophages (CD206+), **(H, R)** M1 macrophages (CD206-, MHCII+ and/or CD80+), **(I, S)** dendritic cells (CD45+, F480-, CD11c+, MHCII+), **(J, T)** activated dendritic cells (CD80+) and analyzed by flow cytometry. Tumours were dissociated and stained for **(K, U)** dendritic cells (CD45+, F480-, CD11c+, MHCII+), and **(L, V)** activated dendritic cells and analyzed by flow cytometry. Results were analyzed by one-way ANOVA with Tukey's multiple comparisons test; * $p<0.05$, ** $p<0.01$, *** $p<0.001$, **** $p<0.0001$.

Supplemental Figure 4: Fes deficient improves dendritic cell TLR signaling and increases sensitivity to LPS stimulation. Bone marrow derived dendritic cells (BMDCs) were isolated from either *fes*$^{+/+}$ or *fes*$^{-/-}$ mice and stimulated with 1µg/mL for the indicated time points and probed by immunoblot for phospho-NFκB, phospho-TBK1, and GAPDH. Densitometry was performed using ImageJ and normalized to the highest density of the *fes*$^{+/+}$ BMDCs for **(B)** pNFκB and **(C)** pTBK1. Bone marrow derived macrophages (BMDMs) were stimulated with the indicated concentrations of LPS for 120 minutes, and probed by immunoblot for phospho-NFκB, and phospho-TBK1 with densitometry normalized to the 27ng/mL well of *fes*$^{+/+}$ BMDMs.

Supplemental Figure 5: Fes-deficiency confers increased cytokine secretion. Bone marrow derived macrophages (BMDMs) from either *fes*$^{+/+}$ (n=5) or *fes*$^{-/-}$ mice (n=5) were stimulated with 1µg/mL for the indicated times. Supernatants were collected and then pelleted at 10,000rpm at 4ºC for 15 minutes to pellet any cell debris, and assessed for **(A)** CCL2, **(B)** GM-CSF, **(C)** IFNγ, **(D)** IL-1α, **(E)** IL-1β, **(F)** IL-10, **(G)** IL-17A, **(H)** IL-23, and **(I)** IL-27 secretion using the BioLegend Mouse Inflammation LEGENDplex panel. Results were analyzed by two-way

ANOVA with Sidak's multiple comparisons test; * $p<0.05$, ** $p<0.01$, *** $p<0.001$, **** $p<0.0001$.

Supplemental Figure 6: Fes-deficiency confers improving T cell priming capabilities to bone marrow derived macrophages. Bone marrow derived macrophages isolated from either *fes*$^{+/+}$ (n=9), or *fes*$^{-/-}$ (n=9) were pulsed with **(B)** 10^{-9}M, **(C)** 10^{-11}M, **(D)** 10^{-12}M, or **(E)** no SIINFEKL peptide for 2 hours, washed, stimulated with 1µg/mL LPS for 1 hour. Following another wash, OT-1 T cells were added to the macrophage culture in a 1:1 ratio for a total of 6 hours, with 5µg/mL Brefeldin A added after 2 hours. Cells were then analyzed for intracellular IFNγ positivity. **(F)** BMDMs were pulsed with 10^{-10}M SIINFEKL for 2 hours, washed, stimulated with 1µg/mL LPS for 7 hours or left untreated. Cells were then stained for SIINFEKL loaded onto MHC-I (*fes*$^{+/+}$ n=5, *fes*$^{-/-}$ n=5). Results were analyzed by two-way ANOVA with Tukey's multiple comparisons test; * $p<0.05$, ** $p<0.01$, *** $p<0.001$, **** $p<0.0001$.

Methods and Materials

Cells and cell culture conditions:

E0771 (CRL-3461), and 293T (CRL-3216) were purchased from the American Type Culture Collection (ATCC, Manassas, VA). B16F10 (CRL-6475) were a gift from Dr. Charles Graham (Kingston, Ontario, Canada). E0771, B16F10 and 293T cells were cultured in Dulbecco's Modified Eagle Medium (DMEM; Gibco cat#: 12100-061) supplemented with 10% fetal bovine serum (FBS; Corning Cat#:35-077-CV) 2mM L-glutamine (Corning; cat#:25-005-CI), and 1% antibiotic and antimycotics (A/A. Gibco; cat#:15240-062). Cell lines were cultured in an incubator held at 5% CO_2 and 37□. Cells used in all experiments were determined to be mycoplasma negative by the mycoplasma PCR detection kit (Applied Biological Materials; cat# G238).

Generation of bone marrow derived macrophages and dendritic cells:

Bone marrow derived macrophages (BMDMs) were isolated similarly to described previously(62, 63)In brief, on day 1, *fes*$^{+/+}$ or *fes*$^{-/-}$ (18)C57BL/6 mice (8 – 12 weeks old) were sacrificed and bone marrow flushed from both tibias and femurs in 5mL of Roswell Park Memorial Institute (RPMI) 1640 (Sigma-Aldrich; cat#:R8758-500mL) supplemented with 2% FBS and 1% A/A. Isolated bone marrow was resuspend by passing through a 23-gauge needle. Cells were passed through a 40µm cell strainer and pelleted at 1000rpm for 5 minutes. Cells were then resuspended in BMDM media (RPMI 1640 supplemented with 15% FBS, 1% A/A, 50µM α-monothioglycerate (α-MTG; Sigma; cat#:M-1753), and 20ng/mL macrophage colony-stimulating factor (M-CSF; a generous gift from Richard Stanley)(64)) and plated in 100mm cell culture plates. On day 2, non-adherent cells were collected, and pelleted at 1000rpm for 5 minutes. Cells were resuspended in 6mL of BMDM media (3mL fresh media and 3mL of conditioned media from previous day) and plated on a 60mm cell culture plate. On Day 4, non-adherent cells were collected, pelleted, resuspended in 10mL of BMDM media, and plated onto untreated tissue culture plates. After 72 hours, cells were trypsonized, counted, and used for downstream experiments.

Pattern recognition signaling cascade immunoblotting analysis

BMDMs from *fes*$^{+/+}$ and *fes*$^{-/-}$ mice were plated in 6-well flat bottom TC-treated plates (Corning, USA) at 2,500,000 cells per well in 2mL of complete macrophage media. The BMDMs were either left untreated or were stimulated with 1µg/mL LPS (Sigma-Aldrich, USA) for 15, 30, 45, or 60 minutes. Cells were washed twice with ice-cold phosphate buffered saline (PBS; 170mM NaCl, 3.5mM KCl, 10mM Na_2HPO_4, 2mM KH_2PO_4, pH 7.2) supplemented with 2mM sodium orthovanadate (ThermoFisher Scientific cat#: 205330500) and lysed in RIPA buffer (10 mM Tris pH7.2, 158 mM NaCl, 1 mM EDTA, 0.1% SDS, 1% Na Deoxycholate, 1% Triton-100) supplemented with Halt™ Protease Inhibitor Cocktail (ThermoFisher Scientific cat#: 87785) and sodium orthovanadate or in 2x Laemmli Buffer for looking at pIRF3. Protein quantification was performed using the Pierce™ BCA Protein Assay Kit (ThermoFisher Scientific cat#: 23225) and immunoblotting was performed as previously described(65) using the following antibodies and concentrations: Fes (1:1000; Cell Signaling Technologies cat#: 85704S), phospho-NF-κB (1:1000; Cell Signaling Technologies cat#: 3033S), , phospho-TBK1 (1:1000; Cell Signaling Technologies cat#: 5483), phospho-SHP2 (1:1000; Cell Signaling Technologies cat#:5431s), phospho-IRF3 (1:1000; Cell Signaling Technologies cat#:29047S), γ-tubulin (1:1000; Sigma-Millipore, cat#: T5326), and GAPDH (1:10000; Cell Signaling Technologies cat#: 5174S).

RNA sequencing

BMDMs from *fes*$^{+/+}$ and *fes*$^{-/-}$ mice were plated in 6-well flat bottom TC-treated plates (Corning, USA) at 2,500,000 cells per well in 2mL of complete macrophage media. The BMDMs were either left untreated, or they were stimulated with 1µg/mL LPS (Sigma-Aldrich, USA) for 4 hours. Cells were then lysed with 350µL of cold TRI Reagent® (Sigma-Aldrich, USA) for five minutes. RNA purification was performed according to Invitrogen's TrizolTM Regent protocol. Purified RNA sample concentrations were determined with a NanoDrop ND-1000 spectrophotometer for downstream cDNA synthesis. cDNA synthesis was carried out using the Maxima First Strand cDNA synthesis kit (Thermo Fisher Scientific, USA) according to manufacturer's instructions, with 372ng of RNA as the starting template. Samples were mixed, centrifuged, and placed in an Applied Biosystems thermocycler (Life Technologies, USA) for one cycle for 10 minutes at 25°C, 15 minutes at 50°C and finally 5 minutes at 85°C. RNA quality and quantity were confirmed via NanoDrop measurement. All samples possessed an A260/280 purity ratio >1.7 and were sent to Genome Quebec (Montreal, Canada) for poly-A enriched RNA-sequencing. Genome Quebec conducted an alignment of the sequencing data to the GRCm38 (Ensembl 102 release) murine genome to determine raw expression gene counts and transcripts per million (TPM) counts. The data was then pre-processed by removing genes with zero counts across all samples and filtering out genes with expression levels below the 75th percentile threshold (roughly 12 counts). The resulting pre-processed TPM counts for each gene were plotted for each genotype condition.

LEGENDplex cytokine assay

BMDMs from *fes*$^{+/+}$ and *fes*$^{-/-}$ mice were plated in 6-well flat bottom TC-treated plates (Corning, USA) at 2,500,000 cells per well in 2mL**.** BMDMs were either left untreated, or they were stimulated with 1µg/mL LPS (Sigma-Aldrich, USA) in 1mL for 4 hours, 8 hours, or 12 hours. Supernatant was then collected, and spun at 10,000rpm for 12 minutes at 4ºC to pellet cell debris. Supernatant was then used in the Mouse Inflammation LEGENDplex panel (BioLegend; cat #: 740446) according to manufacturer's instructions.

Macrophage and T cell coculture:

BMDMs were harvested as described above and were seeded in a 96-well plate. BMDMs were then treated for 2 hours with varying concentrations of OVA peptide (SIINFEKL: CPC Scientific cat#: MISC-012). BMDMs were then washed three times with serum free RPMI, before treatment with1µg/mL of Lipopolysaccharides (LPS; *E. coli*, serotype 055:B5, Sigma Aldrich cat#: L2637), for 1 hour. BMDMs were then washed three times again with serum free RPMI. Spleens from OT-1 mice were isolated, manually dissociated, filtered through a 40µm filter, and subjected to a CD8^{+} T cell negative selection with the EasySep^{TM} Mouse T cell isolation kit (STEMCELL Technologies cat#: 19853), according to the manufacturer's protocol. Isolated CD8^{+} T cells were seeded onto treated BMDMs in a ratio of 1:1 resuspended in T cell media (RPMI 1640, 10% FBS, 1% A/A, 1% gentamicin (ThermoFisher Scientific cat#: 15710064) and incubated for 2 hours after which cells were treated with 1x Brefeldin A (BioLegend; cat#: 420601) and incubated for a final 4 hours before analysis by flow cytometry for T cell activation.

Animal Studies:

All experiments involving the use of animals were performed in accordance with the Canadian Council on Animal Care guidelines and with the approval of Queen's University Animal Care Committee. All mouse strains (*fes*$^{KR/KR}$(66), *fes*$^{-/-}$ (18)and OT-1 (C57BL/6-Tg(TcraTcrb)1100Mjb/J, https://www.jax.org/strain/003831) were on a C57BL/6 background. Mice were bred in-house and 8–12-week-old males or females were used in engraftment studies for B16F10 or E0771 models, respectively with drug and antibody doses normalized to body weights. Animals were randomized at treatment start time, with any mice lacking tumour growth excluded from the study. Tumour length (*L*) and width (*W*) were measured by caliper, and tumour volume calculated with the following formula: (L x W^{2})/2. Tumours were measured until an endpoint of 1.1cm^{3} or humane endpoint (e.g., ulceration) at which point mice were euthanized and survival analyzed.

Doxorubicin therapy model:

C57BL/6 mice (8-12 weeks old) were orthotopically engrafted with 1x10^{5} E0771 cells injected into the fourth mammary fat pad with a Hamilton syringe, or with 6x10^{4} B16F10 cells in a 1:1 ratio of Matrigel (Corning cat#: 354234) to PBS cell suspension injected subcutaneously with a 26-gauge needle into the left flank. Once tumours reached ~100mm^{3} (E0771 model: *fes*$^{+/+}$ ~12 days; *fes*$^{-/-}$ ~14 days)(B16F10 model: *fes*$^{+/+}$ ~8 days; *fes*$^{-/-}$ ~10 days), E0771 tumour-bearing mice were treated with either 5mg/kg of Dox (Selleckchem cat#: S120813) or vehicle control in a 200µL 5% DMSO/PBS solution injected intraperitoneally (IP), repeated 5 and 10 days later; or

for the B16F10 model, 2.5mg/kg Dox or vehicle control in a 200µL 5% DMSO/PBS solution injected IP every 2 days to a final cumulative dose of 20mg/kg. Tumour growth and survival were analyzed as described above.

Anti-PD-1 immune checkpoint blockade therapy model:

The anti-PD-1 treatment model followed a similar protocol to that described above; however, every mouse was treated with its tumour-specific Dox dose in combination with either 10mg/kg anti-IgG control antibody (BioXCell; cat#: BE0089) or 10mg/kg anti-PD-1 antibody (BioXCell; cat#:BE0146) IP, for a total of three doses, either with every Dox treatment in the E0771 model or every two Dox treatments starting on the third Dox treatment in the B16F10 model.

Harvesting tumours and spleens for tumour immune profiling

Mice were engrafted with cancer cells and treated as described above. However, three days following the second dose of Dox treatment in the E0771 model, or one day after the fourth dose in the B16F10 model, mice were euthanized, and tumours and spleens harvested. Tumours were cut into ~1mm^3 chunks with a straight razor, and spleens were pressed through a sieve with a syringe plunger. Tumour samples were suspended in RPMI 1640 supplemented with 10% FBS, 1mg/mL collagenase B (Sigma-Aldrich cat#: 11088815001) and 25µg/mL of DNAse I (Sigma-Aldrich Cat#: 10104159001), while spleens were resuspended in RPMI containing only 25µg/mL of DNAse I. Tumour chunks were then transferred into C Tubes (Miltenyi Biotec cat#: 130-096-334) and dissociated using the gentleMACS Dissociator following the manufacturer's protocol for tough (E0771) or soft (B16F10) tumours. Tumour and spleen homogenates were then filtered through a 70µM cell strainer followed by a 40µM cell strainer and then treated with Ammonium Chloride Potassium (ACK) lysis buffer to lyse red blood cells within the preparation. Cells were then washed and resuspended in fluorescence-activated cell sorting (FACS) buffer (PBS containing 0.75% bovine serum albumin (BSA; BioShop cat#: ALB001), 5mM EDTA in PBS) in preparation for flow staining.

Antibody staining and flow cytometry

Once cells of interested were harvested, 1x10^5 cells/well were plated into 96-well round bottom plates and centrifuged at 1000rpm for 5 minutes. Supernatants were carefully decanted, and cell pellets resuspended in 100µL FACS containing 0.2µg TruStain FcX™ (anti-mouse CD16/32) antibody or 100µL of PBS containing 0.2µg TruStain FcX™ and 0.04µL Zombie AquaTM Fixable Viability Kit (BioLegend cat#: 423102) and incubated at room temperature (RT) in the dark for 30 minutes. Next, 200µL of FACS buffer was added to each well, gently mixed, and pelleted at 1000rpm for 5 minutes, and carefully decanted. Next, cells were stained by resuspending in 100µL of FACS buffer containing appropriate antibody panels and incubated on ice in the dark for 30 minutes. 200µL of FACS was added to each well, gently mixed, and pelleted at 1000rpm for 5 minutes, and carefully decanted, followed by an additional wash in 200µL FACS buffer. If the cells were not being subjected to intracellular staining, cells were resuspended in 100µL of 1% paraformaldehyde in PBS and incubated at room temperature for 30 minutes. An additional 200µL of FACS buffer was added, cells pelleted at 1500rpm for 5 minutes, decanted, and resuspended in 200µL FACS buffer to be analyzed on a CytoFlex-S Flow Cytometer (Beckman Coulter). For intracellular staining, cells were stained following the

ThermoFisher "BestProtocols: Staining Intracellular Antigens for Flow Cytometry – Protocol A" using the eBioscience™ Permeabilization Buffer (ThermoFisher Scientific cat#: 00-8333-56) and eBioscience™ IC Fixation Buffer (ThermoFisher Scientific cat#: 00-8222-49) before analysis on the CytoFlex-S Flow Cytometer (Beckman Coulter). Data analysis was performed using FlowJo® v10 software (FlowJo, LLC, Ashland, OR).

Macrophage adoptive transfer:

C57BL/6 *fes*$^{+/+}$ mice (8-12 weeks old) were engrafted with either E0771 or B16F10 cells as described above. BMDMs for adoptive transfer were isolated from 8-12 week old *fes*$^{+/+}$ or *fes*$^{-/-}$ mice as described above, then treated overnight with 20ng/mL interferon gamma (IFN-γ; Peprotech cat#: 315-05) to polarize them into an M1-like state on Day 6. These were harvested and 3x10^{6} *fes*$^{+/+}$ or *fes*$^{-/-}$ M1-polarized BMDMs in 50µL of PBS, or PBS alone were injected intratumourally (IT) with a 26-gauge needle into 100mm^{3} B16F10 tumours. Nine days later, mice were euthanized, and tumour weights determined and in the E0771 model, were then processed for immune profiling.

1. Pardoll DM. The blockade of immune checkpoints in cancer immunotherapy. Nature Reviews Cancer. 2012;12(4):252-64.
2. Postow MA, Callahan MK, Wolchok JD. Immune Checkpoint Blockade in Cancer Therapy. J Clin Oncol. 2015;33(17):1974-82.
3. Zhao X, Subramanian S. Intrinsic Resistance of Solid Tumors to Immune Checkpoint Blockade Therapy. Cancer Research. 2017;77(4):817-22.
4. Andrews LP, Marciscano AE, Drake CG, Vignali DAA. LAG3 (CD223) as a cancer immunotherapy target. Immunological Reviews. 2017;276(1):80-96.
5. Liu J, Chen Z, Li Y, Zhao W, Wu J, Zhang Z. PD-1/PD-L1 Checkpoint Inhibitors in Tumor Immunotherapy. Frontiers in Pharmacology. 2021;12.
6. Khan M, Arooj S, Wang H. NK Cell-Based Immune Checkpoint Inhibition. Front Immunol. 2020;11:167.
7. Zhou J, Wang G, Chen Y, Wang H, Hua Y, Cai Z. Immunogenic cell death in cancer therapy: Present and emerging inducers. Journal of Cellular and Molecular Medicine. 2019;23(8):4854-65.
8. Ahmed A, Tait SWG. Targeting immunogenic cell death in cancer. Molecular Oncology. 2020;14(12):2994-3006.
9. Mirlekar B, Pylayeva-Gupta Y. IL-12 Family Cytokines in Cancer and Immunotherapy. Cancers. 2021;13(2):167.
10. Boukhaled GM, Harding S, Brooks DG. Opposing Roles of Type I Interferons in Cancer Immunity. Annu Rev Pathol. 2021;16:167-98.
11. Lu C, Klement JD, Ibrahim ML, Xiao W, Redd PS, Nayak-Kapoor A, et al. Type I interferon suppresses tumor growth through activating the STAT3-granzyme B pathway in tumor-infiltrating cytotoxic T lymphocytes. Journal for ImmunoTherapy of Cancer. 2019;7(1):157.
12. Curtsinger JM, Lins DC, Mescher MF. Signal 3 Determines Tolerance versus Full Activation of Naive CD8 T Cells. 2003;197(9):1141-51.
13. Zagorulya M, Yim L, Morgan DM, Edwards A, Torres-Mejia E, Momin N, et al. Tissue-specific abundance of interferon-gamma drives regulatory T cells to restrain DC1-mediated priming of cytotoxic T cells against lung cancer. Immunity. 2023;56(2):386-405.e10.

14. Laight BJ, Jawa NA, Tyryshkin K, Maslove DM, Boyd JG, Greer PA. Establishing the role of the FES tyrosine kinase in the pathogenesis, pathophysiology, and severity of sepsis and its outcomes. Frontiers in Immunology. 2023;14.
15. Salvi V, Gianello V, Tiberio L, Sozzani S, Bosisio D. Cytokine Targeting by miRNAs in Autoimmune Diseases. Frontiers in Immunology. 2019;10.
16. Fajgenbaum DC, June CH. Cytokine Storm. New England Journal of Medicine. 2020;383(23):2255-73.
17. Haigh J, McVeigh J, Greer P. The fps/fes tyrosine kinase is expressed in myeloid, vascular endothelial, epithelial, and neuronal cells and is localized in the trans-golgi network. Cell Growth Differ. 1996;7(7):931-44.
18. Zirngibl RA, Senis Y, Greer PA. Enhanced Endotoxin Sensitivity in Fps/Fes-Null Mice with Minimal Defects in Hematopoietic Homeostasis. Molecular and Cellular Biology. 2002;22(8):2472-86.
19. Parsons SA, Greer PA. The Fps/Fes kinase regulates the inflammatory response to endotoxin through down-regulation of TLR4, NF-κB activation, and TNF-α secretion in macrophages. Journal of Leukocyte Biology. 2006;80(6):1522-8.
20. Xu S, Liu X, Bao Y, Zhu X, Han C, Zhang P, et al. Constitutive MHC class I molecules negatively regulate TLR-triggered inflammatory responses via the Fps–SHP-2 pathway. Nature Immunology. 2012;13(6):551-9.
21. Chen RY, Zhu Y, Shen YY, Xu QY, Tang HY, Cui NX, et al. The role of PD-1 signaling in health and immune-related diseases. Front Immunol. 2023;14:1163633.
22. Hanahan D, Weinberg Robert A. Hallmarks of Cancer: The Next Generation. Cell. 2011;144(5):646-74.
23. Zirngibl R, Schulze D, Mirski SEL, Cole SPC, Greer PA. Subcellular Localization Analysis of the Closely Related Fps/Fes and Fer Protein-Tyrosine Kinases Suggests a Distinct Role for Fps/Fes in Vesicular Trafficking. Experimental Cell Research. 2001;266(1):87-94.
24. Zhang S, Chitu V, Stanley ER, Elliott BE, Greer PA. Fes Tyrosine Kinase Expression in the Tumor Niche Correlates with Enhanced Tumor Growth, Angiogenesis, Circulating Tumor Cells, Metastasis, and Infiltrating Macrophages. Cancer Research. 2011;71(4):1465-73.
25. Muller WJ, Sinn E, Pattengale PK, Wallace R, Leder P. Single-step induction of mammary adenocarcinoma in transgenic mice bearing the activated c-neu oncogene. Cell. 1988;54(1):105-15.
26. Karamanavi E, McVey DG, van der Laan SW, Stanczyk PJ, Morris GE, Wang Y, et al. The FES Gene at the 15q26 Coronary-Artery-Disease Locus Inhibits Atherosclerosis. Circ Res. 2022;131(12):1004-17.
27. Kleffel S, Posch C, Barthel SR, Mueller H, Schlapbach C, Guenova E, et al. Melanoma Cell-Intrinsic PD-1 Receptor Functions Promote Tumor Growth. Cell. 2015;162(6):1242-56.
28. Tomita M, Yasui H, Higashikawa K, Nakajima K, Takakura H, Shiga T, et al. Anti PD-1 treatment increases [18F]FDG uptake by cancer cells in a mouse B16F10 melanoma model. EJNMMI Research. 2018;8(1).
29. Waaler J, Mygland L, Tveita A, Strand MF, Solberg NT, Olsen PA, et al. Tankyrase inhibition sensitizes melanoma to PD-1 immune checkpoint blockade in syngeneic mouse models. Communications Biology. 2020;3(1).
30. Nakamura T, Sato T, Endo R, Sasaki S, Takahashi N, Sato Y, et al. STING agonist loaded lipid nanoparticles overcome anti-PD-1 resistance in melanoma lung metastasis via NK cell activation. Journal for ImmunoTherapy of Cancer. 2021;9(7):e002852.
31. Borchmann S, Selenz C, Lohmann M, Ludwig H, Gassa A, Brägelmann J, et al. Tripartite antigen-agnostic combination immunotherapy cures established poorly immunogenic tumors. Journal for ImmunoTherapy of Cancer. 2022;10(10):e004781.

32. Wculek SK, Amores-Iniesta J, Conde-Garrosa R, Khouili SC, Melero I, Sancho D. Effective cancer immunotherapy by natural mouse conventional type-1 dendritic cells bearing dead tumor antigen. Journal for ImmunoTherapy of Cancer. 2019;7(1).
33. Coussens LM, Werb Z. Inflammation and cancer. Nature. 2002;420(6917):860-7.
34. Greten FR, Grivennikov SI. Inflammation and Cancer: Triggers, Mechanisms, and Consequences. Immunity. 2019;51(1):27-41.
35. Zhao H, Wu L, Yan G, Chen Y, Zhou M, Wu Y, Li Y. Inflammation and tumor progression: signaling pathways and targeted intervention. Signal Transduction and Targeted Therapy. 2021;6(1):263.
36. Gonzalez H, Hagerling C, Werb Z. Roles of the immune system in cancer: from tumor initiation to metastatic progression. Genes Dev. 2018;32(19-20):1267-84.
37. Liu T, Zhang L, Joo D, Sun SC. NF-κB signaling in inflammation. Signal Transduct Target Ther. 2017;2:17023-.
38. Migone TS, Zhang J, Luo X, Zhuang L, Chen C, Hu B, et al. TL1A is a TNF-like ligand for DR3 and TR6/DcR3 and functions as a T cell costimulator. Immunity. 2002;16(3):479-92.
39. Papadakis KA, Prehn JL, Landers C, Han Q, Luo X, Cha SC, et al. TL1A synergizes with IL-12 and IL-18 to enhance IFN-gamma production in human T cells and NK cells. J Immunol. 2004;172(11):7002-7.
40. Twohig JP, Marsden M, Cuff SM, Ferdinand JR, Gallimore AM, Perks WV, et al. The death receptor 3/TL1A pathway is essential for efficient development of antiviral $CD4^+$ and $CD8^+$ T-cell immunity. Faseb j. 2012;26(8):3575-86.
41. Vonderheide RH. CD40 Agonist Antibodies in Cancer Immunotherapy. Annual Review of Medicine. 2020;71(1):47-58.
42. Liu P-S, Chen Y-T, Li X, Hsueh P-C, Tzeng S-F, Chen H, et al. CD40 signal rewires fatty acid and glutamine metabolism for stimulating macrophage anti-tumorigenic functions. Nature Immunology. 2023;24(3):452-62.
43. Labi V, Erlacher M. How cell death shapes cancer. Cell Death & Disease. 2015;6(3):e1675-e.
44. Nössing C, Ryan KM. 50 years on and still very much alive: 'Apoptosis: a basic biological phenomenon with wide-ranging implications in tissue kinetics'. British Journal of Cancer. 2023;128(3):426-31.
45. Akhter N, Takeda Y, Nara H, Araki A, Ishii N, Asao N, Asao H. Apurinic/Apyrimidinic Endonuclease 1/Redox Factor-1 (Ape1/Ref-1) Modulates Antigen Presenting Cell-mediated T Helper Cell Type 1 Responses. The Journal of biological chemistry. 2016;291(45):23672-80.
46. Chiaruttini G, Piperno GM, Jouve M, De Nardi F, Larghi P, Peden AA, et al. The SNARE VAMP7 Regulates Exocytic Trafficking of Interleukin-12 in Dendritic Cells. Cell Rep. 2016;14(11):2624-36.
47. Sangrar W, Shi C, Mullins G, LeBrun D, Ingalls B, Greer PA. Amplified Ras-MAPK signal states correlate with accelerated EGFR internalization, cytostasis and delayed HER2 tumor onset in Fer-deficient model systems. Oncogene. 2015;34(31):4109-17.
48. Gaynor N, Crown J, Collins DM. Immune checkpoint inhibitors: Key trials and an emerging role in breast cancer. Seminars in Cancer Biology. 2022;79:44-57.
49. Wolchok JD, Chiarion-Sileni V, Gonzalez R, Grob J-J, Rutkowski P, Lao CD, et al. Long-Term Outcomes With Nivolumab Plus Ipilimumab or Nivolumab Alone Versus Ipilimumab in Patients With Advanced Melanoma. Journal of Clinical Oncology. 2022;40(2):127-37.
50. Long GV, Stephen Hodi F, Lipson EJ, Schadendorf D, Ascierto PA, Matamala L, et al. Overall Survival and Response with Nivolumab and Relatlimab in Advanced Melanoma. NEJM Evidence. 2023;2(4).
51. Larkin J, Chiarion-Sileni V, Gonzalez R, Grob J-J, Rutkowski P, Lao CD, et al. Five-Year Survival with Combined Nivolumab and Ipilimumab in Advanced Melanoma. New England Journal of Medicine. 2019;381(16):1535-46.

52. Adams S, Schmid P, Rugo HS, Winer EP, Loirat D, Awada A, et al. Pembrolizumab monotherapy for previously treated metastatic triple-negative breast cancer: cohort A of the phase II KEYNOTE-086 study. Ann Oncol. 2019;30(3):397-404.
53. Adams S, Loi S, Toppmeyer D, Cescon DW, De Laurentiis M, Nanda R, et al. Pembrolizumab monotherapy for previously untreated, PD-L1-positive, metastatic triple-negative breast cancer: cohort B of the phase II KEYNOTE-086 study. Annals of Oncology. 2019;30(3):405-11.
54. Nanda R, Chow LQ, Dees EC, Berger R, Gupta S, Geva R, et al. Pembrolizumab in Patients With Advanced Triple-Negative Breast Cancer: Phase Ib KEYNOTE-012 Study. J Clin Oncol. 2016;34(21):2460-7.
55. Tolaney SM, Kalinsky K, Kaklamani VG, D'Adamo DR, Aktan G, Tsai ML, et al. Eribulin Plus Pembrolizumab in Patients with Metastatic Triple-Negative Breast Cancer (ENHANCE 1): A Phase Ib/II Study. Clinical cancer research : an official journal of the American Association for Cancer Research. 2021;27(11):3061-8.
56. Schmid P, Cortes J, Pusztai L, McArthur H, Kümmel S, Bergh J, et al. Pembrolizumab for Early Triple-Negative Breast Cancer. New England Journal of Medicine. 2020;382(9):810-21.
57. Voorwerk L, Slagter M, Horlings HM, Sikorska K, van de Vijver KK, de Maaker M, et al. Immune induction strategies in metastatic triple-negative breast cancer to enhance the sensitivity to PD-1 blockade: the TONIC trial. Nature Medicine. 2019;25(6):920-8.
58. Crosby EJ, Wei J, Yang XY, Lei G, Wang T, Liu CX, et al. Complimentary mechanisms of dual checkpoint blockade expand unique T-cell repertoires and activate adaptive anti-tumor immunity in triple-negative breast tumors. Oncoimmunology. 2018;7(5):e1421891.
59. John LB, Devaud C, Duong CPM, Yong CS, Beavis PA, Haynes NM, et al. Anti-PD-1 Antibody Therapy Potently Enhances the Eradication of Established Tumors By Gene-Modified T Cells. Clinical Cancer Research. 2013;19(20):5636-46.
60. Perez-Lanzon M, Carbonnier V, Cordier P, De Palma FDE, Petrazzuolo A, Klein C, et al. New hormone receptor-positive breast cancer mouse cell line mimicking the immune microenvironment of anti-PD-1 resistant mammary carcinoma. Journal for ImmunoTherapy of Cancer. 2023;11(6):e007117.
61. Zou HY, Li Q, Engstrom LD, West M, Appleman V, Wong KA, et al. PF-06463922 is a potent and selective next-generation ROS1/ALK inhibitor capable of blocking crizotinib-resistant ROS1 mutations. Proc Natl Acad Sci U S A. 2015;112(11):3493-8.
62. Stanley ER. Murine Bone Marrow-Derived Macrophages. In: Pollard JW, Walker JM, editors. Basic Cell Culture Protocols. Totowa, NJ: Humana Press; 1997. p. 301-4.
63. Weischenfeldt J, Porse B. Bone Marrow-Derived Macrophages (BMM): Isolation and Applications. Cold Spring Harbor Protocols. 2008;2008(12):pdb.prot5080.
64. Ladner MB, Martin GA, Noble JA, Wittman VP, Warren MK, McGrogan M, Stanley ER. cDNA cloning and expression of murine macrophage colony-stimulating factor from L929 cells. Proc Natl Acad Sci U S A. 1988;85(18):6706-10.
65. Hoskin V, Ghaffari A, Laight BJ, Sengupta S, Madarnas Y, Nicol CJB, et al. Targeting the Ezrin Adaptor Protein Sensitizes Metastatic Breast Cancer Cells to Chemotherapy and Reduces Neoadjuvant Therapy–induced Metastasis. Cancer Research Communications. 2022;2(6):456-70.
66. Senis Y, Zirngibl R, McVeigh J, Haman A, Hoang T, Greer PA. Targeted disruption of the murine fps/fes proto-oncogene reveals that Fps/Fes kinase activity is dispensable for hematopoiesis. Mol Cell Biol. 1999;19(11):7436-46.

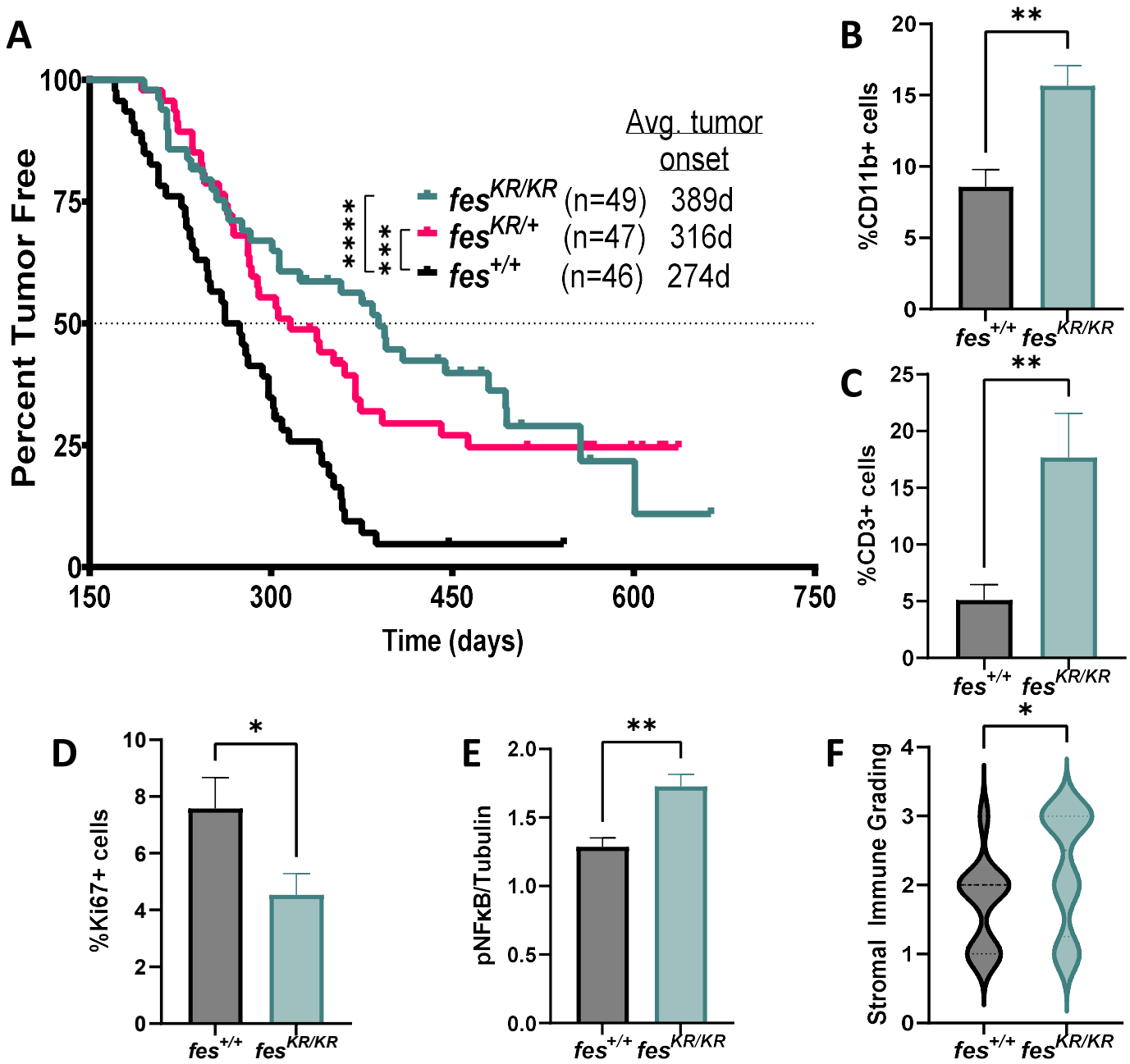
A
Percent Tumor Free
100
75
50
25
0
150
300
450
600
750
Time (days)
Avg. tumor onset
fesKR/KR (n=49) 389d
fesKR/+ (n=47) 316d
fes+/+ (n=46) 274d
***
**
B
%CD11b+ cells
**
fes+/+
fesKR/KR
C
%CD3+ cells
**
D
%Ki67+ cells
*
E
pNFκB/Tubulin
**
F
Stromal Immune Grading
*

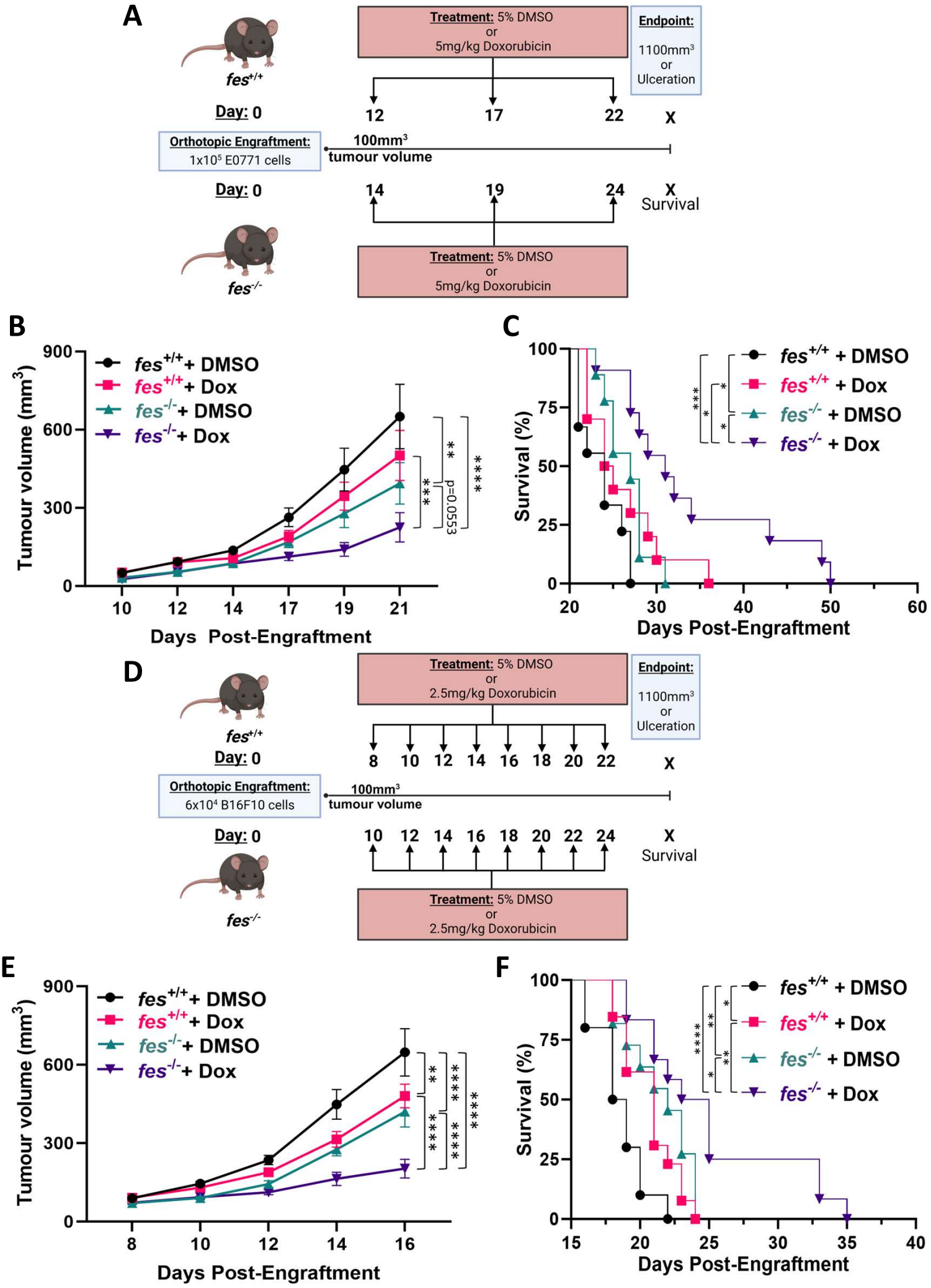
A
fes+/+
Day: 0
Orthotopic Engraftment:
1x10⁵ E0771 cells
Day: 0
fes-/-
Treatment: 5% DMSO
or
5mg/kg Doxorubicin
Endpoint:
1100mm³
or
Ulceration
12
17
22
X
100mm³
tumour volume
14
19
24
X
Survival
Treatment: 5% DMSO
or
5mg/kg Doxorubicin
B
Tumour volume (mm³)
fes+/+ + DMSO
fes+/+ + Dox
fes-/- + DMSO
fes-/- + Dox
p=0.0553
Days Post-Engraftment
C
Survival (%)
fes+/+ + DMSO
fes+/+ + Dox
fes-/- + DMSO
fes-/- + Dox
Days Post-Engraftment
D
fes+/+
Day: 0
Orthotopic Engraftment:
6x10⁴ B16F10 cells
Day: 0
fes-/-
Treatment: 5% DMSO
or
2.5mg/kg Doxorubicin
Endpoint:
1100mm³
or
Ulceration
8
10
12
14
16
18
20
22
X
100mm³
tumour volume
10
12
14
16
18
20
22
24
X
Survival
Treatment: 5% DMSO
or
2.5mg/kg Doxorubicin
E
Tumour volume (mm³)
fes+/+ + DMSO
fes+/+ + Dox
fes-/- + DMSO
fes-/- + Dox
Days Post-Engraftment
F
Survival (%)
fes+/+ + DMSO
fes+/+ + Dox
fes-/- + DMSO
fes-/- + Dox
Days Post-Engraftment

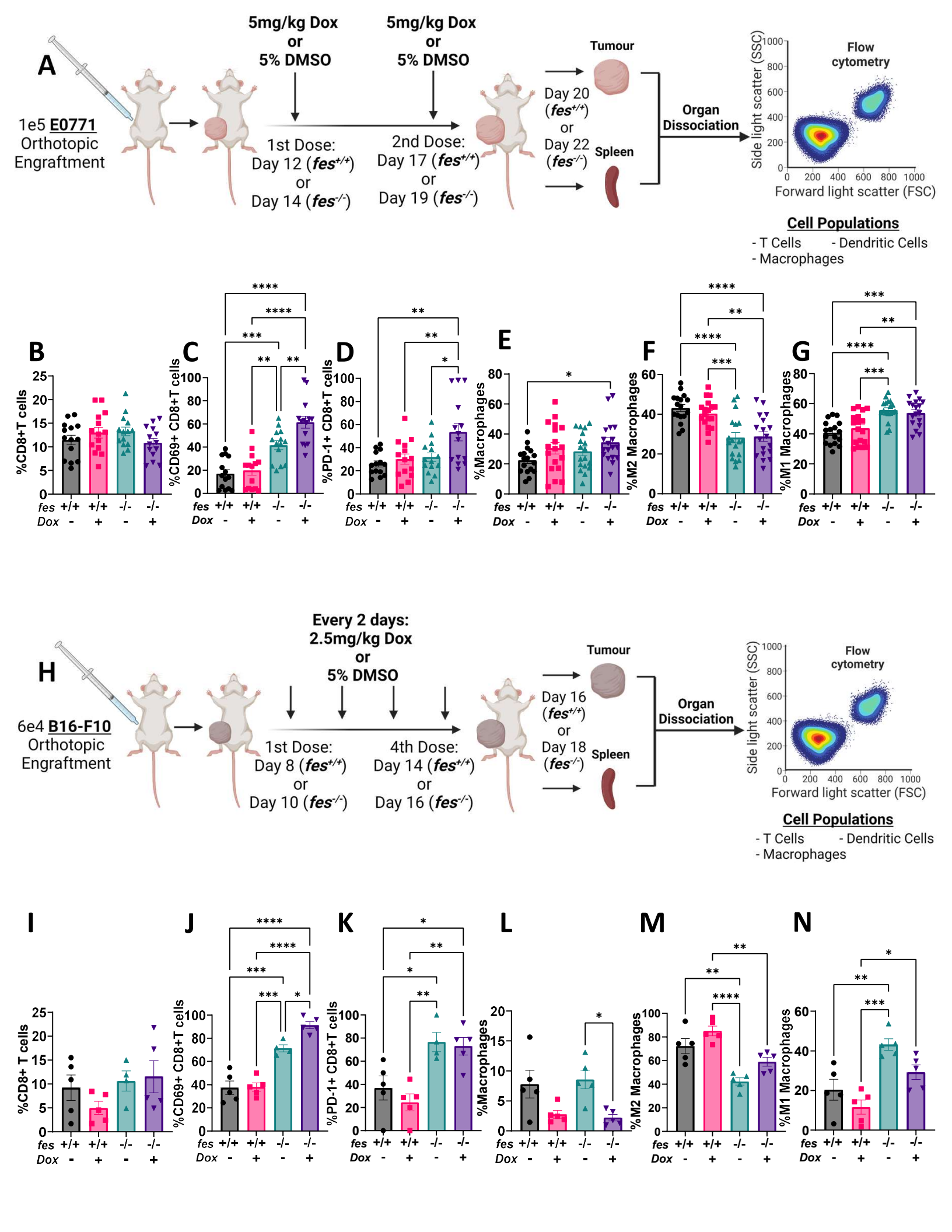
A
1e5 E0771
Orthotopic
Engraftment
5mg/kg Dox
or
5% DMSO
1st Dose:
Day 12 (fes+/+)
or
Day 14 (fes-/-)
5mg/kg Dox
or
5% DMSO
2nd Dose:
Day 17 (fes+/+)
or
Day 19 (fes-/-)
Tumour
Day 20
(fes+/+)
or
Day 22
(fes-/-)
Spleen
Organ
Dissociation
Flow
cytometry
Side light scatter (SSC)
Forward light scatter (FSC)
Cell Populations
- T Cells
- Dendritic Cells
- Macrophages
B
%CD8+T cells
C
%CD69+ CD8+T cells
D
%PD-1+ CD8+T cells
E
%Macrophages
F
%M2 Macrophages
G
%M1 Macrophages
fes +/+ +/+ -/- -/-
Dox - + - +
H
6e4 B16-F10
Orthotopic
Engraftment
Every 2 days:
2.5mg/kg Dox
or
5% DMSO
1st Dose:
Day 8 (fes+/+)
or
Day 10 (fes-/-)
4th Dose:
Day 14 (fes+/+)
or
Day 16 (fes-/-)
Tumour
Day 16
(fes+/+)
or
Day 18
(fes-/-)
Spleen
Organ
Dissociation
Flow
cytometry
Side light scatter (SSC)
Forward light scatter (FSC)
Cell Populations
- T Cells
- Dendritic Cells
- Macrophages
I
%CD8+ T cells
J
%CD69+ CD8+T cells
K
%PD-1+ CD8+T cells
L
%Macrophages
M
%M2 Macrophages
N
%M1 Macrophages
fes +/+ +/+ -/- -/-
Dox - + - +

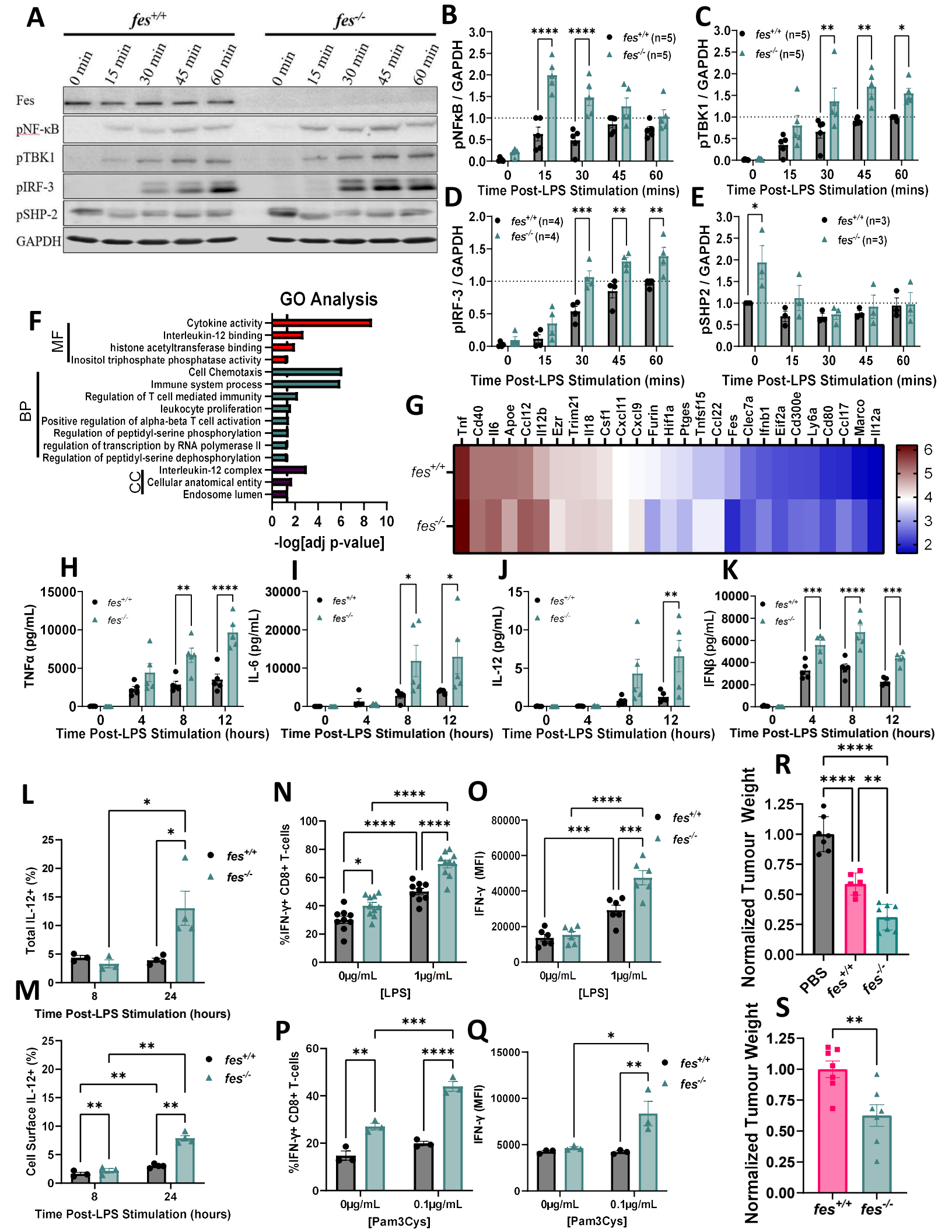
A
fes+/+
fes-/-
0 min
15 min
30 min
45 min
60 min
Fes
pNF-κB
pTBK1
pIRF-3
pSHP-2
GAPDH
B
pNFκB / GAPDH
fes+/+ (n=5)
fes-/- (n=5)
Time Post-LPS Stimulation (mins)
C
pTBK1 / GAPDH
D
pIRF-3 / GAPDH
fes+/+ (n=4)
fes-/- (n=4)
E
pSHP2 / GAPDH
fes+/+ (n=3)
fes-/- (n=3)
F
GO Analysis
MF
Cytokine activity
Interleukin-12 binding
histone acetyltransferase binding
Inositol triphosphate phosphatase activity
BP
Cell Chemotaxis
Immune system process
Regulation of T cell mediated immunity
leukocyte proliferation
Positive regulation of alpha-beta T cell activation
Regulation of peptidyl-serine phosphorylation
regulation of transcription by RNA polymerase II
Regulation of peptidyl-serine dephosphorylation
CC
Interleukin-12 complex
Cellular anatomical entity
Endosome lumen
-log[adj p-value]
G
Tnf
Cd40
Il6
Apoe
Ccl12
Il12b
Ezr
Trim21
Il18
Csf1
Cxcl11
Cxcl9
Furin
Hif1a
Ptges
Tnfsf15
Ccl22
Fes
Clec7a
Ifnb1
Eif2a
Cd300e
Ly6a
Cd80
Ccl17
Marco
Il12a
H
TNFα (pg/mL)
Time Post-LPS Stimulation (hours)
I
IL-6 (pg/mL)
J
IL-12 (pg/mL)
K
IFNβ (pg/mL)
L
Total IL-12+ (%)
M
Cell Surface IL-12+ (%)
N
%IFN-γ+ CD8+ T-cells
[LPS]
0μg/mL
1μg/mL
O
IFN-γ (MFI)
P
[Pam3Cys]
0.1μg/mL
Q
R
Normalized Tumour Weight
PBS
S

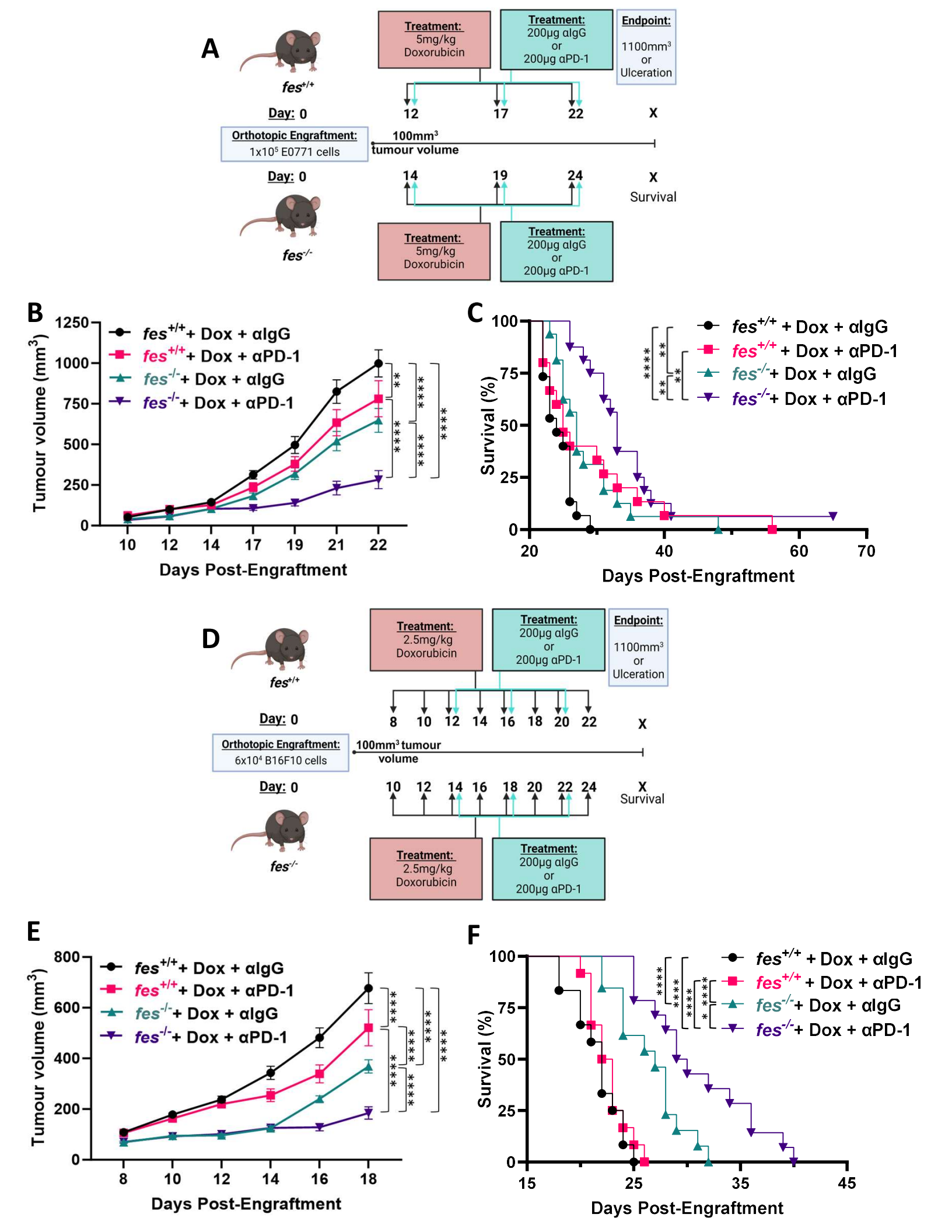
A
fes+/+
Day: 0
Treatment: 5mg/kg Doxorubicin
Treatment: 200µg αIgG or 200µg αPD-1
Endpoint: 1100mm³ or Ulceration
12
17
22
X
Orthotopic Engraftment: 1x10⁵ E0771 cells
100mm³ tumour volume
Day: 0
14
19
24
X
Survival
fes-/-
Treatment: 5mg/kg Doxorubicin
Treatment: 200µg αIgG or 200µg αPD-1
B
Tumour volume (mm³)
fes+/+ + Dox + αIgG
fes+/+ + Dox + αPD-1
fes-/- + Dox + αIgG
fes-/- + Dox + αPD-1
Days Post-Engraftment
C
Survival (%)
fes+/+ + Dox + αIgG
fes+/+ + Dox + αPD-1
fes-/- + Dox + αIgG
fes-/- + Dox + αPD-1
Days Post-Engraftment
D
fes+/+
Day: 0
Treatment: 2.5mg/kg Doxorubicin
Treatment: 200µg αIgG or 200µg αPD-1
Endpoint: 1100mm³ or Ulceration
8 10 12 14 16 18 20 22
X
Orthotopic Engraftment: 6x10⁴ B16F10 cells
100mm³ tumour volume
Day: 0
10 12 14 16 18 20 22 24
X
Survival
fes-/-
Treatment: 2.5mg/kg Doxorubicin
Treatment: 200µg αIgG or 200µg αPD-1
E
Tumour volume (mm³)
fes+/+ + Dox + αIgG
fes+/+ + Dox + αPD-1
fes-/- + Dox + αIgG
fes-/- + Dox + αPD-1
Days Post-Engraftment
F
Survival (%)
fes+/+ + Dox + αIgG
fes+/+ + Dox + αPD-1
fes-/- + Dox + αIgG
fes-/- + Dox + αPD-1
Days Post-Engraftment